Journal of University of Science and Technology Beijing
Vol.7(2000), No.4, p.305

Information

Analytical Criteria for Local Activity of CNN with Two-port and Application to Biochemical Model

Lequan Min, Na Yu

Applied Science School, University of Science and Technology Beijing, Beijing 100083, China
(Received 2000-08-25)

Abstract: The analytic criteria are presented for the local activity theory in two-port Cellular Neural Network (CNN) cells with three local state variables, and the application to a Biochemical Model CNN (BMCNN) is given for coupling in series of two enzymes whose prototype was studied by Decroly and Goldbeter. The bifurcation diagrams of the BMCNN's show that there does not exist a locally passive domain, and the computer simulation exhibited that convergent patterns, oscillatory patterns or chaotic patterns may emerge if the selected cell parameters are located in locally active unstable domains but nearby the edge of chaos domain. In particular, the coexistence of multiple oscillations was observed in the corresponding triple cell couples of the BMCNN's with the same initial conditions.

Key words: cellular neural network; local activity; biochemical model; periodicity; chaos

Nonlinear phenomena exist universally in the nature and the society. However the complex dynamics of the corresponding nonlinear models are very difficulty to be studied. The recent local activity theory [1, 2] asserts whether a homogeneous medium is capable of exhibiting complexity depends on whether the CNN cells, or its couplings, is locally active in a precise circuit-theoretic sense, in particular the corresponding CNN cell parameters are located nearby edge of chaos [3, 4]. The analytic criteria for testing the local activity theory with one-port and 1, 2, 3, or 4 state variables have been respectively presented and successfully applied to the research on complex patterns and structure generated from several CNN's with important background [1–5].

In this paper, a set of theorems for testing the locally activity of the CNN's with three state variables and two-port are set up. As an application of the theorems, (1) the biochemical model for coupling in series of two enzyme reaction with autocatalytic regulation [6, 7] is mapped into the BMCNN; (2) the bifurcation diagram of the BMCNN has been draw based on the new theorems which showed that there exist only locally active domains and edge of chaos with respect to the equilibrium points with chemical sense; and (3) the computer simulated both of the original biochemical models and the BMCNN's, which were shown many complex periodic or chaotic trajectories (or patterns). This research demonstrates once again the effectiveness of the local activity theory in choosing the parameters for the emergence of complex (static and dynamic) patterns in a homogeneous lattice formed by coupled locally active cells.

1 Local Activity Theory

For a two-port CNN cell, the corresponding local state equations with "3" state variables assume the form

$$\dot{\boldsymbol{V}}_a=\boldsymbol{A}_{aa}\boldsymbol{V}_a+\boldsymbol{A}_{ab}\boldsymbol{V}_b+\boldsymbol{I}_a \tag{1}$$

$$\dot{\boldsymbol{V}}_b=\boldsymbol{A}_{ba}\boldsymbol{V}_a+\boldsymbol{A}_{bb}\boldsymbol{V}_b \tag{2}$$

where,

$\boldsymbol{V}_a=[V_1, V_2]^T$, $\boldsymbol{V}_b=V_3$, $\boldsymbol{I}_a=[I_1, I_2]^T$

$$\boldsymbol{A}_{aa}=\begin{bmatrix}a_{11} & a_{12}\\ a_{21} & a_{22}\end{bmatrix}, \boldsymbol{A}_{bb}=\begin{bmatrix}a_{13}\\ a_{23}\end{bmatrix}, \boldsymbol{A}_{ba}=[a_{31}, a_{32}], \boldsymbol{A}_{bb}=[a_{33}] \tag{3}$$

The corresponding CNN cell impedance $\boldsymbol{Z}_Q(s)$ is given by [1]

$$\boldsymbol{Z}_Q^{-1}(s)=\boldsymbol{Y}_Q(s)=(s\boldsymbol{I}-\boldsymbol{A}_{aa})-\boldsymbol{A}_{ab}(s\boldsymbol{I}-\boldsymbol{A}_{bb})^{-1}\boldsymbol{A}_{ba}$$
$$=\begin{bmatrix}s-a_{11}-\dfrac{a_{13}a_{31}}{s-a_{33}} & -a_{12}-\dfrac{a_{13}a_{32}}{s-a_{33}}\\ -a_{21}-\dfrac{a_{23}a_{31}}{s-a_{33}} & s-a_{22}-\dfrac{a_{23}a_{32}}{s-a_{33}}\end{bmatrix} \tag{4}$$

Lemma 1.1 ([1]) A two-port reaction diffusion CNN cell is locally active at a cell equilibrium point $Q \triangleq (\bar{V}_1, \bar{I}_1)$ if, and only if, its cell impedance $\boldsymbol{Y}_Q(s)$ at Q satisfies at least one of the following 4 conditions:

(1) $\boldsymbol{Y}_Q(s)$ has a pole in Re $[s]>0$.

(2) $\boldsymbol{Y}_Q^H(i\omega)=\boldsymbol{Y}_Q^\dagger(i\omega)+\boldsymbol{Y}_Q(i\omega)$ is not a positive semi-definite matrix at some $\omega=\omega_0$, where ω_0 is any real number.

(3) $\boldsymbol{Y}_Q(s)$ has a simple pole $s=i\omega_p$ on the imaginary axis, where its associated residue matrix

$$k_1 \triangleq \begin{cases}\lim\limits_{s\to i\omega_p}(s-i\omega_p)\boldsymbol{Y}_Q(s), \text{ if } \omega_p<\infty\\ \lim\limits_{\omega_p\to\infty}\boldsymbol{Y}_Q(i\omega_p)/i\omega_p, \text{ if } \omega_p=\infty\end{cases} \tag{5}$$

is either not a Hermitian matrix, or else not a positive semi-definite Hermitian matrix.

(4) $Y_Q(s)$ has a multiple pole on the imaginary axis.

Where $Y_Q^t(s)$ is constructed by first taking the transpose of $Y_Q(s)$, and then followed by the complex conjugate operation.

2 Theorems for testing the conditions in Lemma 1.1

Firstly, let us recall some lemmas (for example, see reference [8] or other standard functional analysis textbooks).

Lemma 2.1 If $X^T Y_Q^H(s)X$ for $\forall X\in\mathbb{C}$ is real then $Y_Q^H(s)$ must be a self-adjoint operator from $\mathbb{C}^n\longrightarrow\mathbb{C}^n$.

Proof See Theorem 3.10-3 in reference [8].

Lemma 2.2 If $Y_Q^H(s)$ is not a self-adjoint operator from $\mathbb{C}^n\longrightarrow\mathbb{C}^n$ then $Y_Q^H(s)$ is not a positive semi-definite matrix.

Lemma 2.3 If $Y_Q^{H\dagger}(s)=Y_Q^H(s)$ and $Y_Q^H(s)$ is not a positive semi-definite matrix at some $i\omega=i\omega_0\in i\mathbb{R}$, if, and only if, there is at least one $\lambda<0$ s.t. $\lambda\in\sigma(Y_Q^H(i\omega))$.

Proof Since from Theorem 9.2-1 in reference [8], it is known that for any bounded self-adjoint linear operator T: $\boldsymbol{H}\to\boldsymbol{H}$ on a Hilbert space $\boldsymbol{H}$,

$$\min_{\lambda\in\sigma(T)}=\inf_{\|x\|=1}\langle Tx,x\rangle,\quad \max_{\lambda\in\sigma(T)}=\sup_{\|x\|=1}\langle Tx,x\rangle.$$

This completes the proof.

Using the above lemmas and the methods similar to those stated in reference [4], the following theorems can be proved.

Theorem 2.1 $Y_Q(s)$ has a pole in Re $[s]>0$ if, and only if, $a_{33}>0$ and $\max\{|a_{13}a_{31}|,|a_{13}a_{32}|,|a_{23}a_{31}|,|a_{23}a_{32}|\}\neq 0$.

Proof By the definition of pole, formula (4) implies the theorem.

Theorem 2.2 Let $b=a_{13}a_{31}a_{33}$, $e=a_{23}a_{32}a_{33}$, $c=a_{13}a_{32}a_{33}+a_{23}a_{31}a_{33}$, $d=a_{13}a_{31}-a_{23}a_{31}$. $Y_Q(s)$ satisfies condition (2) in Lemma 1.1 if, and only if at least one of the following condition holds.

(1) $(a_{11}+a_{22})>0$;

(2) $(a_{11}+a_{22})\le 0, a_{33}\neq 0$, and $(a_{11}+a_{22})-(a_{13}a_{31}+a_{23}a_{32})/a_{33}>0$;

(3) $4a_{11}a_{22}-(a_{12}+a_{21})^2<0$;

(4) $4(ba_{22}+ea_{11})-2c(a_{12}+a_{21})+d^2\neq 0$,

$$\omega^2=\frac{2a_{33}^2d^2+8be-2c^2}{4(ba_{22}+ea_{11})-2c(a_{12}+a_{21})+d^2}-a_{33}^2>0,$$

$$4\left[a_{11}a_{22}-\frac{ba_{22}+ea_{11}}{a_{33}^2+\omega^2}+\frac{be}{(a_{33}^2+\omega^2)^2}\right]-\left(a_{12}+a_{21}-\frac{c}{a_{33}^2+\omega^2}\right)^2-\frac{\omega^2d^2}{(a_{33}^2+\omega^2)^2}<0;$$

(5) $a_{33}\neq 0$ and $4(a_{11}a_{33}^2-b)(a_{22}a_{33}^2-e)-[(a_{12}+a_{21})a_{33}^2-c]^2<0$;

(6) $a_{33}=0$ and $4be-c^2<0$.

Proof Firstly, from formula (4) we obtain

$$Y_Q^H(s)=\begin{bmatrix} -2a_{11}+\dfrac{2a_{13}a_{31}a_{33}}{a_{33}^2+\omega^2} & -(a_{12}+a_{21})+\dfrac{c+i\omega d}{a_{33}^2+\omega^2} \\ -(a_{12}+a_{21})+\dfrac{c-i\omega d}{a_{33}^2+\omega^2} & -2a_{22}+\dfrac{2a_{23}a_{32}a_{33}}{a_{33}^2+\omega^2}\end{bmatrix} \tag{6}$$

Equation (6) gives that $Y_Q^H(i\omega)$ is a self-adjoint operator. Thus, $Y_Q^H(i\omega)$ is not a positive semi-definite matrix. In this case, the eigenvalue λ of matrix $Y_Q^H(i\omega)$ satisfies equation

$$|\lambda I-Y_Q^H(i\omega)|=\lambda^2+a_1\lambda+a_0=0 \tag{7}$$

where,

$$a_1=2(a_{11}+a_{22})-\frac{2(a_{13}a_{31}a_{33}+a_{23}a_{32}a_{33})}{a_{33}^2+\omega^2} \tag{8}$$

$$a_0=4\left(a_{11}-\frac{b}{a_{33}^2+\omega^2}\right)\left(a_{22}-\frac{e}{a_{33}^2+\omega^2}\right)-\left(a_{12}+a_{21}-\frac{c}{a_{33}^2+\omega^2}\right)^2+\frac{\omega^2d^2}{(a_{33}^2+\omega^2)^2} \tag{9}$$

Consequently, we conclude from Lemma 2.3 that $Y_Q^H(i\omega)$ is not a positive semi-definite matrix at some $\omega=\omega_0$, if, and only if

$$a_1>0 \text{ or } a_0<0 \tag{10}$$

Case 1 Testing condition $a_1>0$.

(1) If $a_{11}+a_{22}>0$, then it follows from equation (8) that if ω is large enough, $a_1>0$. Hence we have

(I) If $a_{11}+a_{22}>0$ then $Y_Q^H(i\omega)$ satisfies condition (2) in Lemma 1.1.

(2) If $a_{11}+a_{22}\le 0$ and $a_{33}(a_{13}a_{31}+a_{23}a_{32})\ge 0$, then $a_1>0$ can not hold for any $\omega\in\mathbb{R}$.

(3) If $a_{11}+a_{22}\le 0$ and $a_{33}(a_{13}a_{31}+a_{23}a_{32})<0$, then $a_1>0$ has a solution $\omega\in\mathbb{R}\Longleftrightarrow a_{11}+a_{22}-a_{33}(a_{13}a_{31}+a_{23}a_{32})/a_{33}^2>0$. Therefore we conclude that

(II) If $a_{11}+a_{22}\le 0$, $a_{33}\neq 0$ and $a_{11}+a_{22}-a_{33}(a_{13}a_{31}+a_{23}a_{32})/a_{33}^2>0$ then $Y_Q^H(i\omega)$ satisfies condition (2) in Lemma 1.1.

Case 2 Testing condition $a_0<0$.

(1) If $4a_{11}a_{12}-(a_{12}+a_{21})^2<0$, then it follows from equation (9) that if ω is large enough, $a_0<0$. Therefore we obtain

(III) If $4a_{11}a_{12}-(a_{12}+a_{21})^2<0$, then $Y_Q^H(i\omega)$ satisfies condition (2) in Lemma 1.1.

(2) If $4a_{11}a_{12}-(a_{12}+a_{21})^2\geq 0$. Let $L(\omega^2)=a_0$.

(A) If $L(0)<0$, we conclude that

(IV) If $4a_{11}a_{12}-(a_{12}+a_{21})^2\geq 0$ and

when $a_{33}\neq 0$,

$4a_{33}^2(a_{11}a_{33}^2-b)(a_{22}a_{33}^2-e)-[(a_{12}+a_{21})a_{33}^2-c]^2<0$;

when $a_{33}=0$,

$4be-c^2<0$.

Then $\boldsymbol{Y}_Q^H(i\omega)$ satisfies condition (2) in Lemma 1.1.

(B) If $L(0)\geq 0$. Since $\lim_{\omega\to\infty} L(\omega^2)=4a_{11}a_{22}-(a_{12}+a_{21})^2\geq 0$, we only need to examine the minum of $L(\omega^2)$ in $[0,+\infty]$. Solving $\dot{L}_{\omega^2}(\omega^2)=0$, we obtain

$4(ba_{22}+ea_{11})(a_{33}^2+\omega^2)-8be-2c(a_{12}+a_{21})(a_{33}^2+\omega^2)+2c^2-d^2(a_{33}^2+\omega^2)+2\omega^2d^2=0$,

$$\omega^{*2}=\frac{2a_{33}^2d^2+8be-2c^2}{4(ba_{22}+ea_{11})-2c(a_{12}+a_{21})+d^2}-a_{33}^2.$$

It follows that

(V) If $\omega^{*2}>0$ and $L(\omega^{*2})<0$, then $\boldsymbol{Y}_Q^H(i\omega)$ satisfies condition (2) in Lemma 1.1.

In summary from (I) to (V), this completes our proof.

Theorem 2.3 $\boldsymbol{Y}_Q(s)$ satisfies condition (3) in Lemma 1.1 if, and only if, at least one of the following condition holds.

(1) If $a_{33}=0$, $\max\{|a_{13}a_{31}|, |a_{13}a_{32}|, |a_{23}a_{31}|, |a_{23}a_{32}|\}\neq 0$, and $a_{13}a_{32}\neq a_{23}a_{31}$.

(2)If $a_{33}=0$; $\max\{|a_{13}a_{31}|, |a_{13}a_{32}|, |a_{23}a_{31}|, |a_{23}a_{32}|\}\neq 0$, $a_{13}a_{32}=a_{23}a_{31}$ and

(a) $a_{13}a_{31}+a_{23}a_{32}>0$ or

(b) $a_{13}a_{31}a_{23}a_{32}-a_{13}^2a_{32}^2<0$.

Proof $\boldsymbol{Y}_Q(s)$ has a simple pole $s=i\omega$ on the imaginary axis $\Longleftrightarrow$ $a_{33}=0$ and $\max\{|a_{13}a_{31}|, |a_{13}a_{32}|, |a_{23}a_{31}|, |a_{23}a_{32}|\}\neq 0$. In this case,

$$k_1=\lim_{s\to 0} s\boldsymbol{Y}_Q(s)=\begin{bmatrix}-a_{13}a_{31} & -a_{13}a_{32}\\ -a_{23}a_{31} & -a_{23}a_{32}\end{bmatrix}.$$

Therefore if $a_{13}a_{32}\neq a_{23}a_{31}$, then $\boldsymbol{Y}_Q(s)$ satisfies condition (3) in Lemma 1.1. On the other hand, if $a_{13}a_{32}=a_{23}a_{31}$, then $\boldsymbol{Y}_Q(s)$ is a Hermitian matrix. Since

$\det|\lambda I-k_1|=\lambda^2+\lambda(a_{13}a_{31}+a_{23}a_{32})+a_{13}a_{31}a_{23}a_{31}-a_{13}^2a_{32}^2$,

if $a_{13}a_{31}+a_{23}a_{32}>0$ or $a_{13}a_{31}a_{23}a_{31}-a_{13}^2a_{32}^2<0$, then $\boldsymbol{Y}_Q(s)$ satisfies condition (3) in Lemma 1.1.

Finally, $\boldsymbol{Y}_Q(s)$ has a simple $i\omega$-axis pole at infinity and

$$\lim_{\omega_p\to\infty}\frac{\boldsymbol{Y}_Q(i\omega_p)}{i\omega_p}=I$$

is a positive-definite matrix.

In summary, this completes the proof.

Theorem 2.4 $\boldsymbol{Y}_Q(s)$ does not have a multiple pole on the imaginary axis.

Proof Equation (4) shows that $\boldsymbol{Y}_Q(s)$ has no a multiple pole on the imaginary axis.

3 BGCNN Equations, Bifurcation Diagrams and Dynamic Simulations

3.1 BGCNN equations

All life is rhythmical. The only way to understand these biological rhythms is to become more quantitative and to develop rigorous mathematical models. As one of the models for glycolytic oscillations that occur in yeast and muscle cells, a three-variable biochemical model for the coupling in series of two enzyme reactions with autocatalytic regulation takes the following form ([6,7]):

$$\frac{d\alpha}{dt}=\nu-\sigma_1\phi(\alpha,\beta),$$

$$\frac{d\beta}{dt}=q_1\sigma_1\phi(\alpha,\beta)-\sigma_2\eta q_1\sigma_1\phi(\alpha,\beta)-\sigma_2\eta(\beta,\gamma),$$

$$\frac{d\gamma}{dt}=q_2\sigma_2\eta(\beta,\gamma)-k_s\gamma \qquad (11)$$

where α, β, γ denote the (dimensionless) normalized concentrations of the substrate S of the first enzyme E_1, the product P_1 transformed by E_1 and the product P_2 transformed by the second enzyme E_2, respectively; L_1 and L_2 are the allosteric constant of enzymes E_1 and E_2, while σ_1 and σ_2 are the normalized maximum rates (in s^{-1}) of the two enzymes; ν and k_s (both in s^{-1}) denote the substrate injection rate and the apparent first-order rate constant for the removal of the final product in a reaction catalyzed by a Michaelian enzyme far from saturation by its substrate; the rate functions ϕ and η of the allosteric enzymes E_1 and E_2 are given by

$$\phi=\frac{\alpha(1+\alpha)(1+\beta)^2}{L_1+(1+\alpha)^2(1+\beta)^2},$$

$$\eta=\frac{\beta(1+\gamma)^2}{L_2+(1+\gamma)^2}.$$

Now we map equation (11) into a standard $N\times 1$ BMCNN array with two-port (with diffusion coefficients D_1 and D_2) described via

$$\frac{d\alpha_i}{dt}=\nu_i-\sigma_1\phi(\alpha_i,\beta_i)+D_1(\alpha_{i-1}+\alpha_{i+1}-2\alpha_i),$$

$$\frac{d\beta_i}{dt}=q_1\sigma_1\phi(\alpha_i,\beta_i)-\sigma_2\eta q_1\sigma_1\phi(\alpha_i,\beta_i)-\sigma_2\eta(\beta_i,\gamma_i)+D_2(\beta_{i-1}+\beta_{i+1}-2\alpha_i),$$

$$\frac{dy_i}{dt}=q_2\sigma_2\eta(\beta_i,\gamma_i)-ks\gamma_i,$$

$$i=1,2,\cdots,50 \tag{12}$$

In component form, equation (12) become

$$\dot{\alpha}=f_1(\alpha,\beta,\gamma)+D_1\nabla^2\alpha \tag{13}$$

$$\dot{\beta}=f_2(\alpha,\beta,\gamma)+D_2\nabla^2\beta \tag{14}$$

$$\dot{\gamma}=f_3(\alpha,\beta,\gamma) \tag{15}$$

where ∇^2 corresponds to a 50×50 matrix.

The cell equilibrium points Q's of equations (13)–(15) can be determined via the following equations:

$$f_1(\alpha,\beta,\gamma)=0 \tag{16}$$

$$f_2(\alpha,\beta,\gamma)=0 \tag{17}$$

$$f_3(\alpha,\beta,\gamma\gamma)=0 \tag{18}$$

To solve equations (16)–(19), the unique cell equilibrium point Q which has biochemical sense is given via

$$Q=(\bar{\alpha},\bar{\beta},\bar{\gamma}) \tag{19}$$

$$\bar{\alpha}=\frac{\sigma_1}{2(\sigma_1-\nu)}-\left[\frac{\sigma_1^2}{4(\sigma_1-\nu)^2}+\frac{\nu L_1}{(\sigma_1-\nu)(1+\beta)^2}\right]^{1/2} \tag{20}$$

$$\bar{\gamma}=\frac{q_1q_2\nu}{ks},\ \bar{\beta}=\frac{ks\gamma[L_2+(1+\gamma)^2]}{q_2\sigma_2(1+\gamma)^2} \tag{21}$$

The cell coefficients $a_{m,n}(Q)$'s are defined via the corresponding Jacobian matrix

$$\boldsymbol{A}\triangleq\begin{bmatrix}a_{11}(Q) & a_{12}(Q) & a_{13}(Q)\\ a_{21}(Q) & a_{22}(Q) & a_{23}(Q)\\ a_{31}(Q) & a_{32}(Q) & a_{33}(Q)\end{bmatrix}\triangleq\begin{bmatrix}\boldsymbol{A}_{aa} & \boldsymbol{A}_{ab}\\ \boldsymbol{A}_{ba} & \boldsymbol{A}_{bb}\end{bmatrix}$$

$$\triangleq\begin{bmatrix}\frac{\partial f_1(\boldsymbol{X})}{\partial\alpha} & \frac{\partial f_1(\boldsymbol{X})}{\partial\beta} & \frac{\partial f_1(\boldsymbol{X})}{\partial\gamma}\\ \frac{\partial f_2(\boldsymbol{X})}{\partial\alpha} & \frac{\partial f_2(\boldsymbol{X})}{\partial\beta} & \frac{\partial f_2(\boldsymbol{X})}{\partial\gamma}\\ \frac{\partial f_3(\boldsymbol{X})}{\partial\alpha} & \frac{\partial f_3(\boldsymbol{X})}{\partial\beta} & \frac{\partial f_3(\boldsymbol{X})}{\partial\gamma}\end{bmatrix} \tag{22}$$

where $\boldsymbol{X}=(\alpha(Q),\beta(Q),\gamma(Q))$. Consequently, the corresponding CNN cell impedance $\boldsymbol{Y}_Q(s)$ can be calculated via equations (22) and (4).

3.2 Bifurcation diagrams

Using Theorems 2.1–2.4 and formulas (4) and (22), the bifurcation diagrams with respect to the equilibrium point Q for the BMCNN can be described via computer programs. These domains for different cell parameters are calculated numerically and shown in **figure 1**, where the fixed cell parameter group $\{\sigma_1, \sigma_2, L_1, L_2\ q_1, q_2\}=\{10,10,5\times10^8,100,50,0.02\}$. Interestingly, the chaotic parameters $\{ks,\nu\}=\{1.4,0.25\}$ and $\{ks,\nu\}=\{2,0.45\}$ calculated in references [6] and [7] are just located nearby the edge of chaos. Most strikingly, there is no locally passive domain in the bifurcation diagrams.

3.3 Dynamic simulations of the GMCNN equations

Firstly let us simulate the original biochemical model because it is easier to be coped with and has the similar properties to those of the corresponding BMCNN equations. The results of simulation are listed in **table 1** and some of the dynamic patterns of the simulation are shown in **figure 2.**

Table 1 tells us that the locally active theory is also a useful tool for studying the complexity of the original biochemical model (11). Interestingly, the parameters $\{k_s, \nu\}$'s are located nearby edge of chaos, chaotic trajectories or period-i limit cycles can be generated. In particular on the line ν=0.2, so-called period-adding phenomenon appears which is firstly observed in a physical system in reference [9,10]. In our case the period-adding bifurcation-period-1, 2, 3, 4 or 5 limit cycles and a chaotic trajectory appear consecutively as the parameter k_s varying in [0.60, 1.48] (see figure 2).

The simulation on the BMCNN's is difficult due to the limit of the memory of Matlab 5.2 software. Even

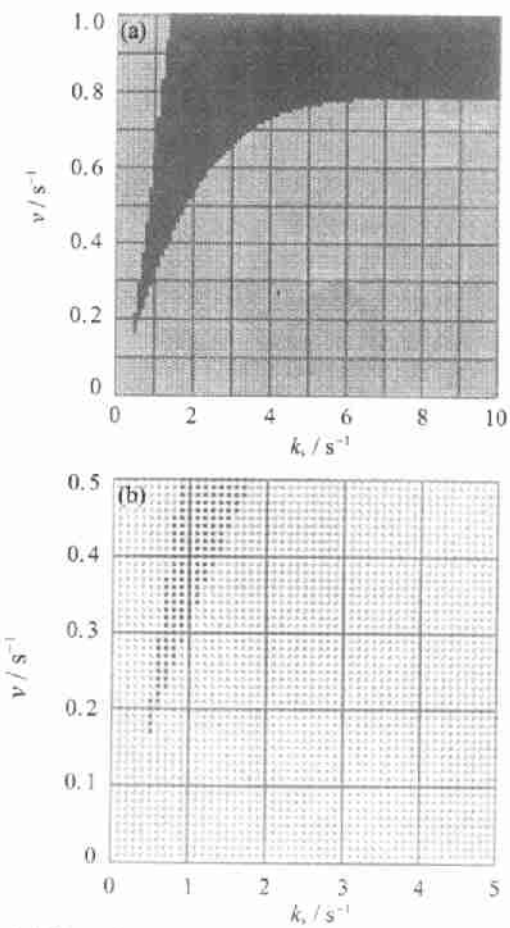

Figure 1 Bifurcation diagram of the BMCNN. The domains are coded as follows: edge of chaos (locally active and stable) domain (black), locally active and unstable domain (gray). (a) at cross-section $k_s\in[0,1]$, and (b) at cross-section $k_s\in[0,5]$ and $\nu\in[0,0.5]$.

Table 1 Cell parameters and corresponding dynamic properties of the enzyme CNN's where σ_1=10, σ_2=10, L_1=5×10^8, L_2=10^2, q_1 =50, and q_2=0.02. The symbols ⇓, ⇑, *j*p and ⊕ indicate that convergent patterns, divergent patterns, *j*-period patterns and chaotic patterns are observed near to or far from the corresponding equilibrium points, respectively.

No.	k_1 / s^{-1}	v / s^{-1}	Cell equilibrium point Q	Eigenvalue	Pattern
1	10.000	0.250	29.053 4, 120.226 8, 0.025 0	−9.512 0, 0.037 6 ± 0.019 7 i	1p
2	1.450	0.250	37.939 1, 92.188 6, 0.172 4	−0.977 8, 0.030 8 ± 0.040 0 i	4p
3	1.400	0.250	38.333 9, 91.240 8, 0.178 6	−0.927 4, 0.030 2 ± 0.041 1 i	⊕
4	1.350	0.250	38.760 0, 90.239 3, 0.185 2	−0.876 9, 0.029 5 ± 0.042 2 i	2p
5*	0.600	0.250	54.999 0, 63.533 7, 0.416 7	−0.042 4, −0.019 8 ± 0.155 1 i	1p⇓
6	0.200	0.250	96.711 0, 31.864 2, 0.800 0	−0.005 2, 0.124 4 ± 0.212 0 i	6p
7	2.000	0.250	34.962 3, 100.015 4, 0.125 0	−1.527 8, 0.034 5 ± 0.032 5 i	8p
8	2.000	0.400	31.693 6, 140.888 9, 0.200 0	−1.276 6, 0.019 2 ± 0.070 3 i	10p
9	0.800	0.250	237.796 3, 26.675 7, 3.200 0	−0.004 0, 0.615 3 ± 0.454 2 i	1p
10	1.821	0.400	32.732 9, 136.447 5, 0.219 7	−1.098 1, 0.016 4 ± 0.073 1 i	1p
11*	1.200	0.400	39.042 5, 114.500 0, 0.333 3	−0.443 3, −0.014 6 ± 0.094 7 i	1p
12	0.200	0.400	180.487 2, 24.222 2, 2.000 0	−0.002 9, 0.369 9 ± 0.319 0 i	1p
13	1.450	0.300	180.487 2, 24.222 2, 2.000 0	−0.002 9, 0.369 9 ± 0.319 0 i	⊕
14	1.500	0.300	36.385 5, 105.666 7, 0.200 0	−0.942 2, 0.025 0 ± 0.054 2 i	⊕
15	1.530	0.300	36.150 6, 106.350 8, 0.196 1	−0.972 4, 0.025 4 ± 0.053 6 i	5p
16	10.000	0.300	26.849 8, 142.889 4, 0.030 0	−9.417 2, 0.034 7 ± 0.034 2 i	2p
17	1.400	0.300	37.247 2, 103.230 1, 0.214 3	−0.840 8, 0.023 0 ± 0.056 6 i	2p
18	1.000	0.300	42.610 1, 90.257 4, 0.300 0	−0.415 9, 0.004 3 ± 0.073 3 i	2p
19	0.800	0.300	47.569 0, 80.838 8, 0.375 0	−0.140 7, −0.036 7 ± 0.106 9 i	2p
20	0.200	0.300	147.909 5, 25.500 0, 1.500 0	−0.003 1, 0.267 3 ± 0.280 1 i	2p
21	0.200	0.200	117.821 8, 26.000 0, 1.000 0	−0.003 5, 0.166 8 ± 0.214 4 i	2p
22*	0.600	0.200	54.351 8, 57.250 0, 0.333 3	−0.147 4, −0.001 6 ± 0.071 3 i	2p
23	0.800	0.200	47.912 6, 65.000 0, 0.250 0	−0.396 0, 0.023 0 ± 0.044 6 i	1p
24	1.400	0.200	40.173 8, 77.562 5, 0.142 9	−1.015 4, 0.035 8 ± 0.020 7 i	2p
25	1.460	0.200	39.767 7, 78.355 2, 0.137 0	−1.075 7, 0.036 2 ± 0.019 3 i	5p
26	1.480	0.200	39.640 0, 78.607 7, 0.135 1	−1.095 7, 0.036 4 ± 0.018 9 i	4p
27	2.000	0.200	37.252 4, 83.644 6, 0.100 0	−1.615 9, 0.038 3 ± 0.008 2 i	8p
28	1.000	0.200	44.224 5, 70.444 4, 0.200 0	−0.608 8, 0.030 4 ± 0.033 4 i	1p
29	1.200	0.200	41.840 1, 74.469 4, 0.166 7	−0.813 5, 0.033 9 ± 0.026 2 i	1p
30	1.300	0.200	40.939 1, 76.111 1, 0.153 8	−0.914 7, 0.035 0 ± 0.023 3 i	2p
31	1.350	0.200	40.541 4, 76.858 5, 0.148 1	−0.965 1, 0.035 4 ± 0.022 0 i	⊕
32	10.000	0.200	32.071 1, 97.116 9, 0.020 0	0.022 1, 0.058 4, −9.607 8	1p
33	2.000	0.450	31.213 8, 152.187 5, 0.225 0	−1.196 0, 0.012 5 ± 0.080 9 i	⊕
34	1.900	0.450	31.816 0, 149.330 1, 0.236 8	−1.096 1, 0.010 5 ± 0.082 7 i	1p
35	2.050	0.450	30.936 5, 153.540 0, 0.219 5	−1.245 8, 0.013 4 ± 0.080 1 i	10p

so some novel phenomena are still observed. They are addressed as follows.

(1) The BMCNN dynamic patterns are generated by the parameter group No. 30. The parameter group is located in the locally active domain and nearby an edge of chaos. The dynamics of the 3-dimensional biochemical model is a period-2 limit cycle (figure 2(b)). However, the one of the corresponding BMCNN changes obviously. After simulation of a long time, the first triple cell $(\alpha_1,\beta_1,\gamma_1)$ converges to a period-1 limit cycle; the second triple cell $(\alpha_1,\beta_1,\gamma_1)$ converges to a period-3 limit cycle. The consecutive triple cells $(\alpha_i,\beta_i,\gamma_i)$ converges to different periods that larger than three until i=14. The following triple cells converges to period-2 limit cycles. The trajectories and the time evolutions of the triples $(\alpha_i,\beta_i,\gamma_i)$'s for i=1, 2, 25, 50 are exhibited in **figure 3**. The time evolutions at specified time of the dynamics of the BMCNN are given in **figures 4 and 5**. It is observed that the transmission of the concentrations along "cell chain" α is smooth. The concentration γ_i is triggered only after the concentration of the corresponding cell β_i reaches its maximum.

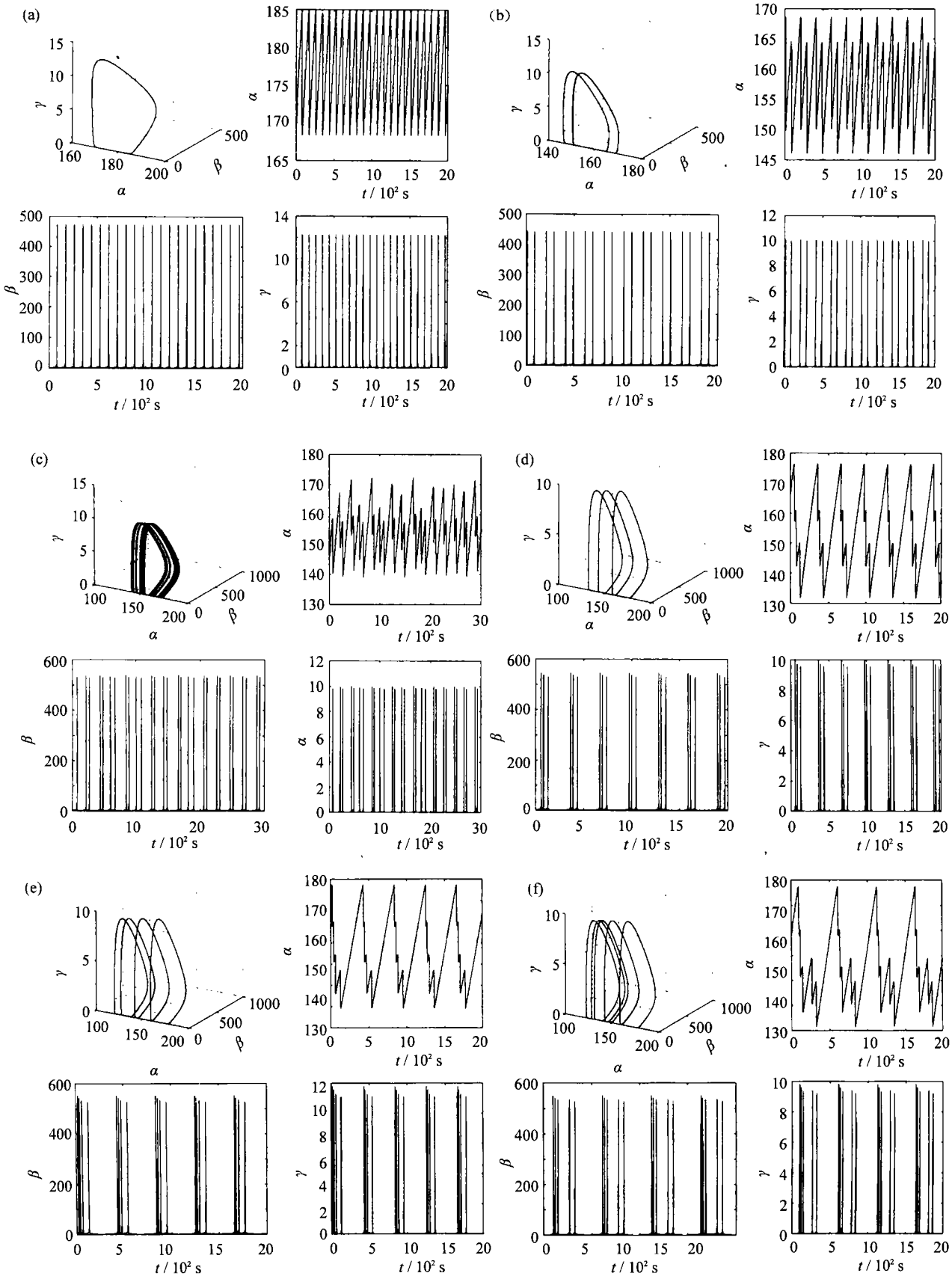

Figure 2 Fixed parameter group $\{\sigma_1,\sigma_2,L_1,L_2,q_1,q_2,v\}$={10, 10, 100, 50, 0.02, 0.2}. The trajectories and the time evolutions of the state variables α, β and γ. Initial condition $X(0)\triangleq[\alpha(0),\beta(0),\gamma(0)]$. (a) Period-1 limit cycle where k_s=0.6 s^{-1} and $X(0)$=[170.1226, 0.1407, 0.0535]; (b) Period-2 limit cycle where k_s=1.3 s^{-1} and $X(0)$=[168.0582, 6.6543, 0.0094]; (c) Chaos k_s=1.35 s^{-1} and $X(0)$=[146.0317, 2.0524, 0.0030]; (d) Period-3 limit cycle where k_s=1.40 s^{-1} and $X(0)$=[166.7481, 1.0294, 0.0014]; (e) Period-4 limit cycle where k_s=1.48 s^{-1} and $X(0)$=[174.3312, 2.1257, 0.0028]; (f) Period-5 limit cycle where k_s=1.46 s^{-1} and $X(0)$=[158.8879, 0.6302, 0.0009].

(2) The BMCNN dynamic patterns are generated by the parameter group No. 31. The parameter group is located in the locally active domain and nearby an edge of chaos. The dynamics of the 3-dimensional biochemical model is chaos (figure2(c)). The one of all triple cell $(\alpha_i,\beta_i,\gamma_i)$'s of the corresponding BMCNN displays chaotic patterns. After long time's simulation, the time evolutions of the triples cell $(\alpha_i,\beta_i,\gamma_i)$'s for i=1, 2, 25, 50 are shown in **figure 6**. The time evolutions at specified time of the dynamics of the BMCNN are described in **figure 7**. It is observed that the transmission of the concentrations along "cell chain" α is abrupt. Some cells in

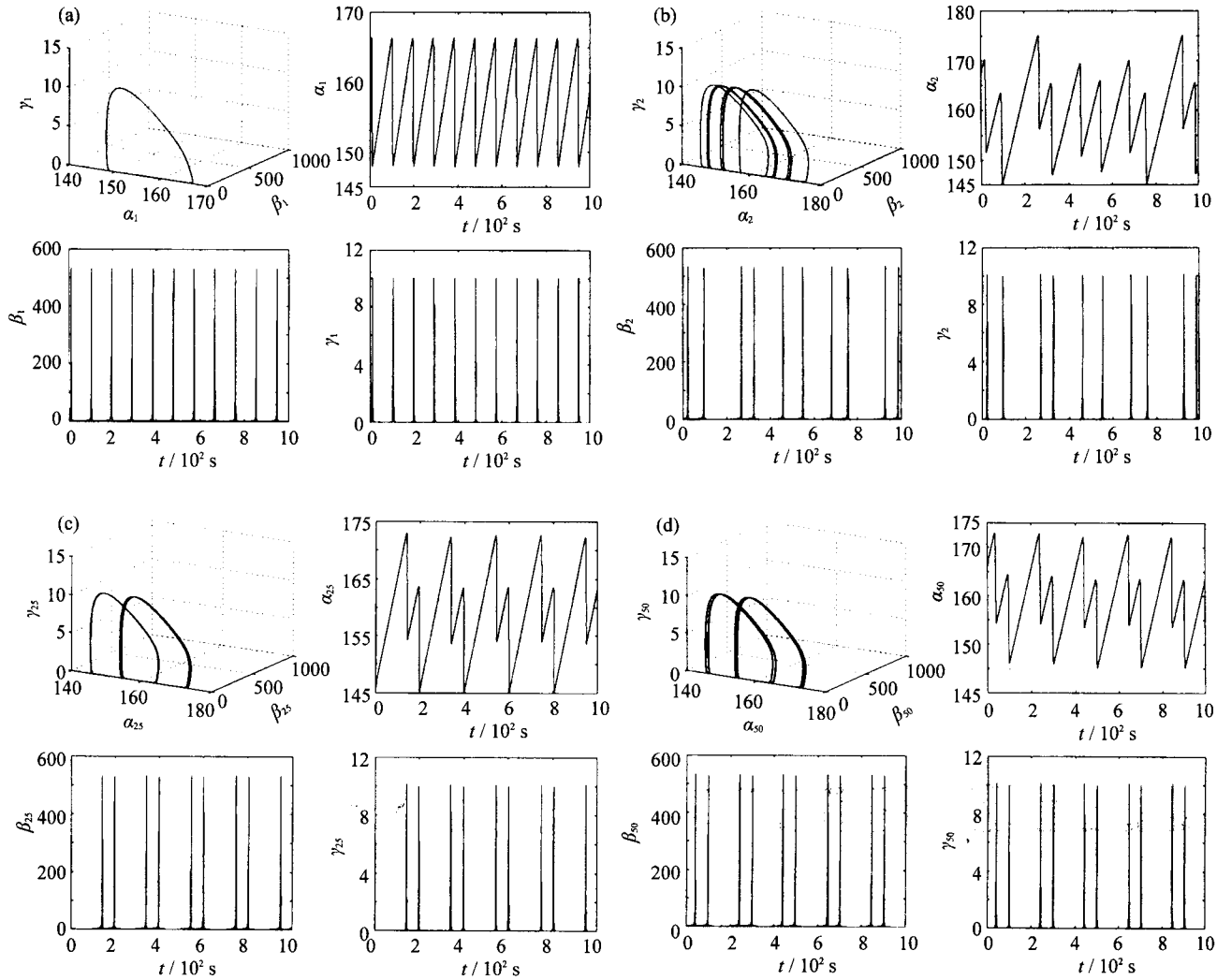

Figure 3 Trajectories and time evolutions of α_i, β_i and γ_i. The parameters are σ_1=10, σ_2=10, L_1=5×10⁸, L_2=100, q_1=50, q_2=0.02, v=0.2 s^{-1}, and k_s=1.35 s^{-1}. (a) i=1; (b) i=2; (c) i=25; (d) i=50.

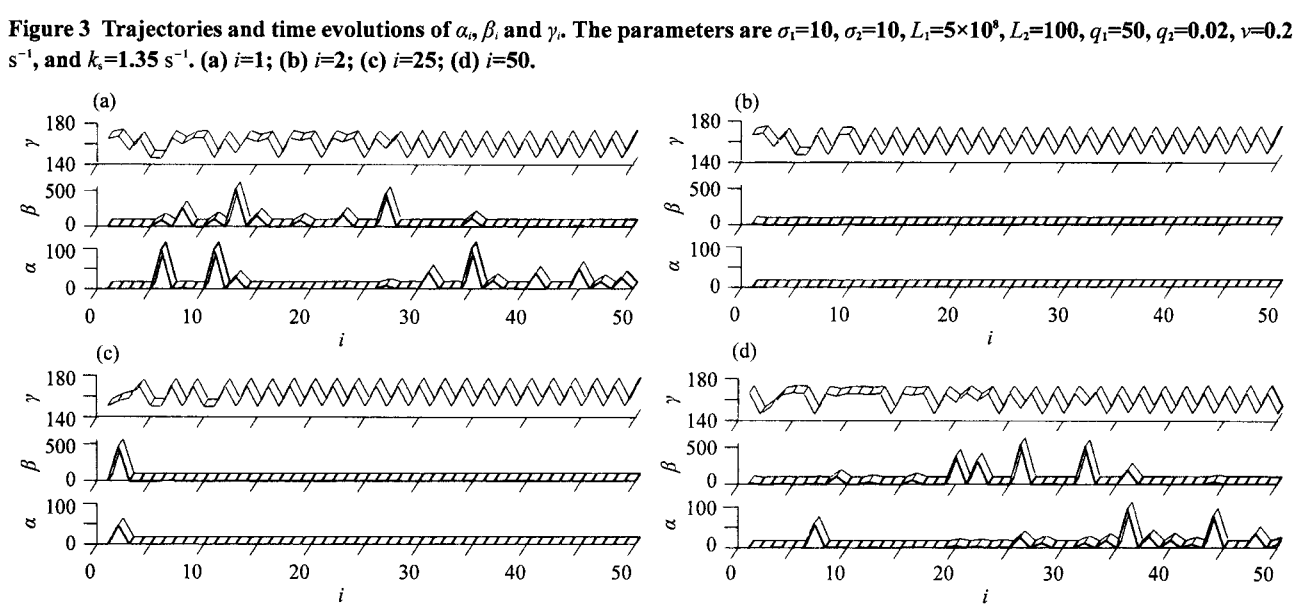

Figure 4 Dynamic patterns of the state variables α, β and γ at the specified time t=0 (a), 6.932 (b), 22.26 (c) and 100.9 s(d).

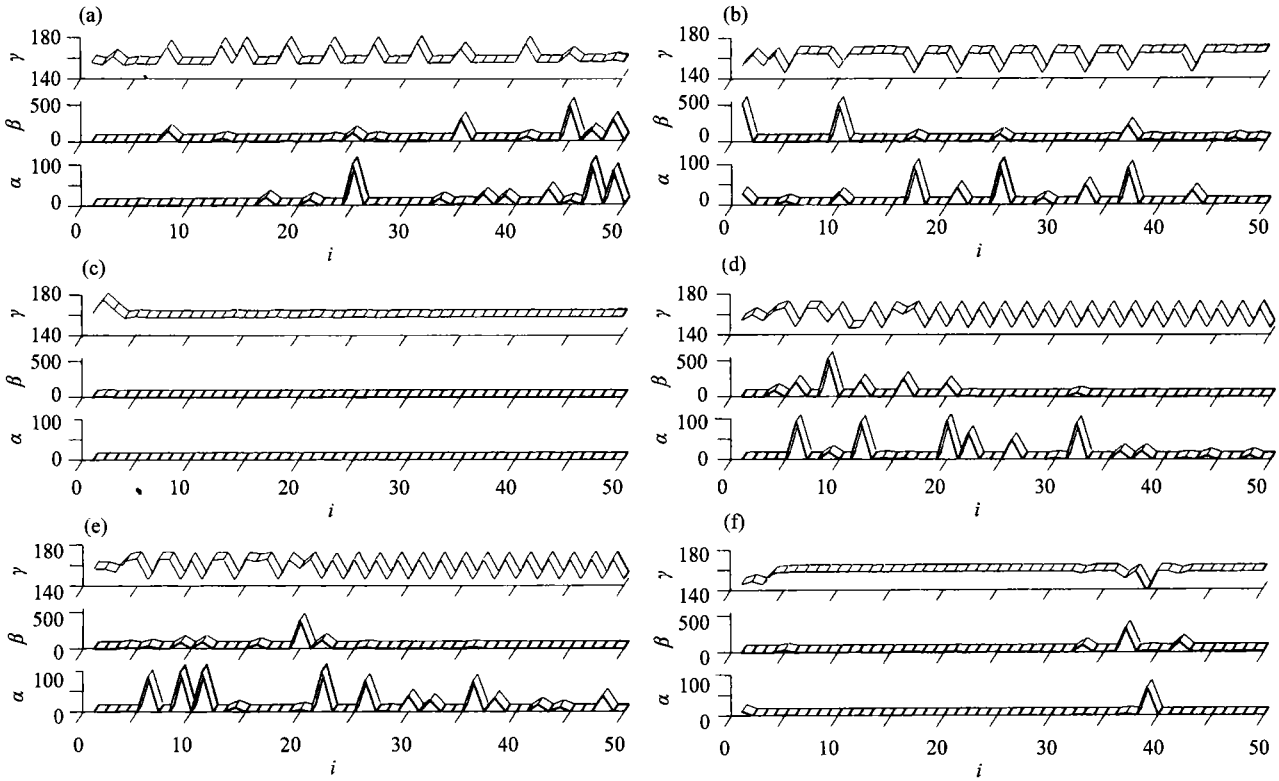

Figure 5 Dynamic patterns of the state variables α, β and γ at the specified time t=142.2 (a), 197.9 (b), 264.5 (c), 507.8 (d), 709.7 (e), and 983.4 s (f).

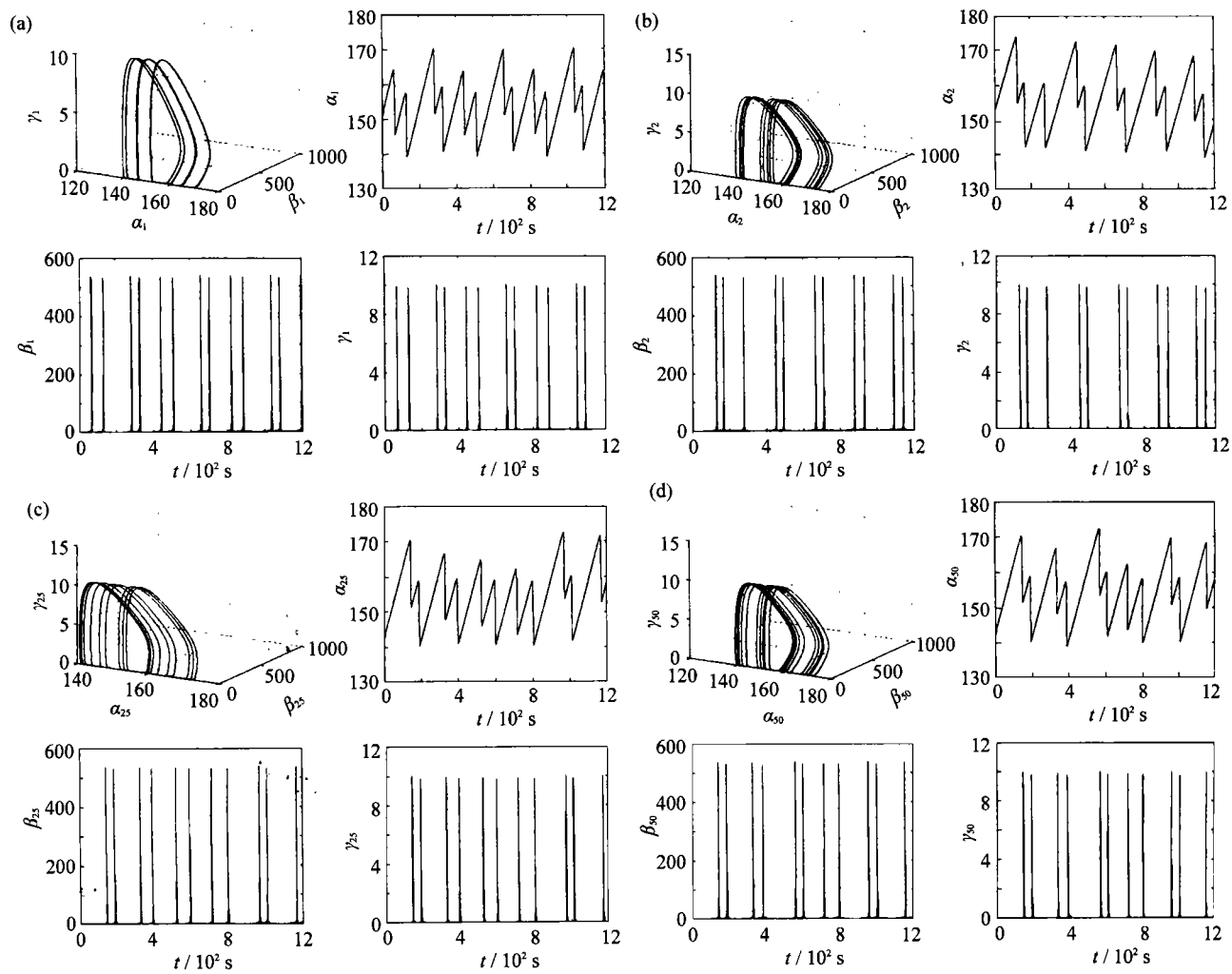

Figure 6 Trajectoies and time evolutions of the state variables α_i, β_i and γ_i. The parameters are σ_1=10, σ_2=10, L_1=5×10⁸, L_2=100, q_1 =50, q_2=0.02, v=0.2 s^{-1}, and k_s=1.35 s^{-1}. (a) i=1; (b) i=2; (c) i=25; (d) i=50.

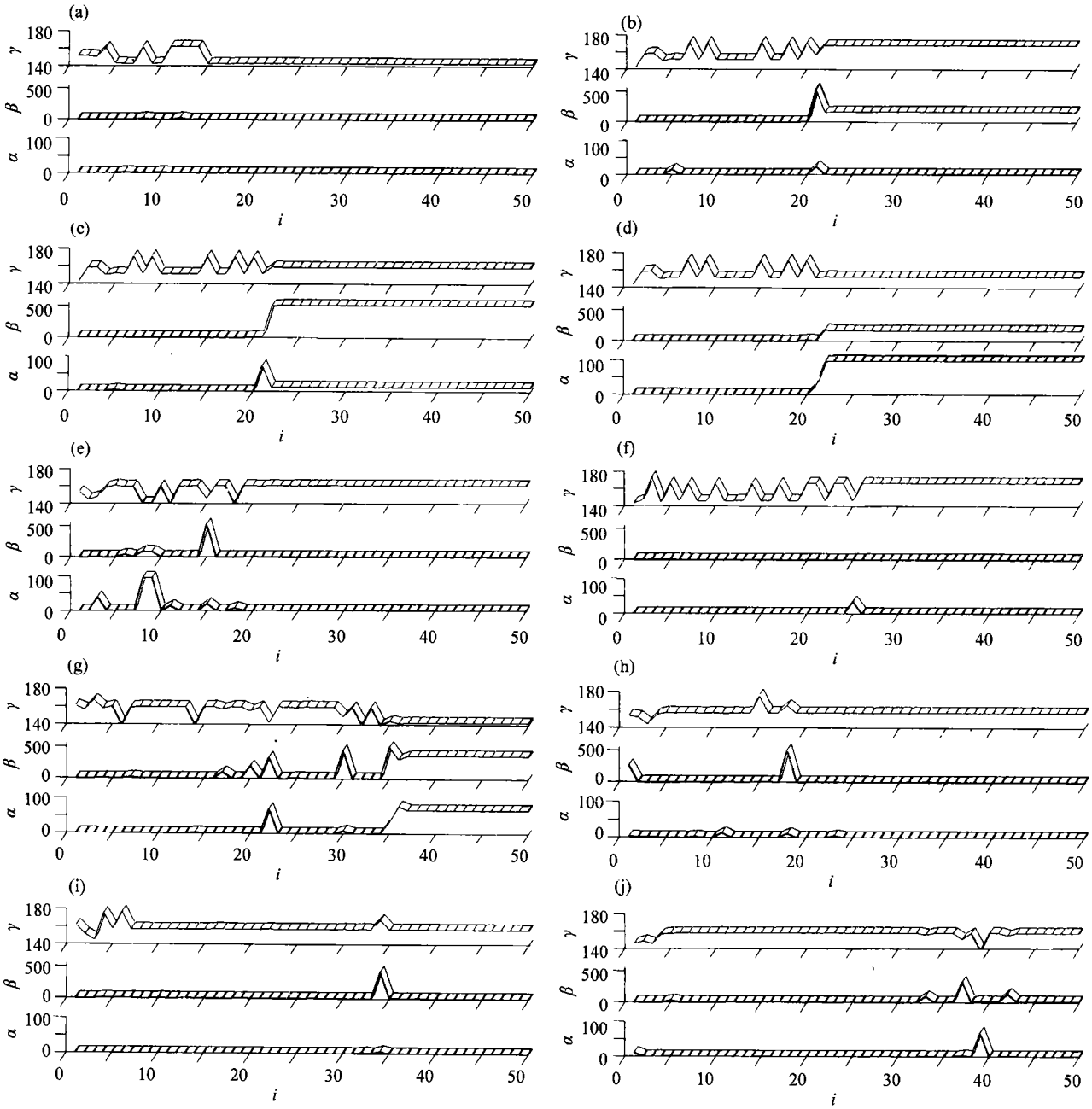

Figure 7 Dynamic patterns of the state variables α, β and γ at the specified time t=0 (a), 145.2 (b), 146.3 (c), 147.1 (d), 293.7 (e), 527.6 (f), 799.0 (g), 884.8 (h), 991.1 (i), and 1 200 s (j).

the chains α, β and γ seem to play the role of pacemaker, that is, they can trigger their all consecutive cells instantly although the concentration γ_i is triggered only after the concentration of the corresponding cell β_i reaches its maximum.

4 Concluding Remarks

The new theorems for testing local activity of the CNN's with three state variables and two-port are presented, which can be used to explore the complex dynamic of general nonlinear equations with 3(state) variables.

The BMCNN equations are introduced whose prototype is the biochemical model describing the glycolytic oscillations that occur in yeast and muscle cells. The bifurcation diagrams of the BMCNN's are calculated based on our theorem and show that there only exist locally active domain and the edge of chaos. The chaotic parameters calculated by references [6, 7] are just located nearby the edge of chaos. Some new chaotic parameters are discovered also near to the edge of chaos.

Extensive numerical simulation discovers that the original biochemical model has the period-adding phenomenon.Multiple periods can coexist in one BMCNN. The transmissions of concentration waves of the periodic BMCNN and chaotic BMCNN are quit different. The former transmits v smoothly but the chaotic one transmits in emergency ways.

In summary, the theorems for testing the local activity presented in this paper are a useful tool for determining the complex behavior of the CNN's. It would be expected that some new results obtained here could get biological explanations.

Acknowledgments

This project is jointly supported by the Foundation for University Key Teachers by the Ministry of Education of China and the Scientific Research Foundation of the University of Science and Technology Beijing.

References

[1] L. O. Chua: *Int. J. Bifurcation and Chaos*, 7(1997), No.10, p. 2219.

[2] L. O. Chua: *IEEE Trans. Circuits Syst. I: Fundamental Theory and Applications*, 46(1999), p.71.

[3] R. Dogaru, L. O. Chua: *Int. J. Bifurcation and Chaos*, 8 (1998), No.2, p.211; No.6, p.1107; No.12, p.2321.

[4] L. Min, K. R. Crounse, L. O. Chua: *Int. J. Bifurcation and Chaos*, 10(2000), No.1, p.25; No.6, p.1295.

[5] L. Min: *J. Univ. Sci. Tech. Beijing*, 7(2000), No.2, p.139.

[6] O. Decroly: Interplay between two periodic enzyme reactions as a source for complex oscillatory behaviour. [In] H. Degen, A. V. Holden, L. F. Olsen, eds. *Chaos in Biological Systems*. Plenum Press, New York and London, 1987, pp.49-58.

[7] A. Goldbeter: *Biochemical oscillations and cellular rhythms: The molecular Bases of periodic andchaotic behavior*. Cambridge University Press, 1996.

[8] E. Kreyszig: *Introduction Functional Analysis with Applications*. John Wiley & Sons, New York, 1978.

[9] L. Q. Pei: IEEE Trans. Circults Syst., 33(1986), No.4, p.438.

[10] L. O. Chua, Y. Yao, Q. Yang: *Int. J. Circuit Theory Applications*, 14 (1986), p.315.